# Transmutation-induced Precipitation in Tungsten Irradiated with A Mixed Energy Neutron Spectrum ♣

Xunxiang Hu [1] *, Chad Parish [1], Kun Wang [1], Takaaki Koyanagi [1], Benjamin P. Eftink [2], Yutai Katoh [1]

[1] Oak Ridge National Laboratory, Oak Ridge, TN 37831, USA

[2] Los Alamos National Laboratory, Los Alamos, NM, 87545, USA

## Abstract

Transmutation-induced precipitation in neutron-irradiated tungsten is an important performance concern for its application as plasma facing material in fusion reactors. In this study, segregation and precipitation of transmutant elements in single crystal and polycrystal tungsten irradiated at 460~1100°C to 0.02~2.4 displacements per atom (dpa) in the High Flux Isotope Reactor were investigated using transmission electron microscopy. The results indicated that nanoscale W-Re-Os clusters were identified in the low dose regime from 0.02 to 0.44 dpa with irradiation temperature lower than 800°C while acicular-shape precipitates formed when irradiation dose is higher than 1.5 dpa. A tentative roadmap of the kinetics process of the transmutation-induced precipitation in neutron-irradiated tungsten is presented characterizing the defect features (i.e., W-Re-Os clusters and precipitates) consisting of transmutant elements in tungsten irradiated to various doses. All TEM-visible voids were associated with the acicular-shape precipitates. Voids were formed prior to the formation of acicular-shape precipitates and act as strong trapping sites for mobile species involved in the precipitation together with dislocations. Thermal stability of W-Re-Os clusters was assessed by performing a 2-h

♣ *Email address of the corresponding author: hux1@ornl.gov

anneal at 1200°C on tungsten irradiated to 0.44 dpa at 705°C. The kinetics process of transmutant elements and radiation defects are discussed to reveal the underlying mechanisms controlling the formation of precipitates in tungsten.

## 1. Introduction

Tungsten (W) has been perceived as the leading candidate material for plasma facing component in ITER and is expected to also be for future fusion reactors. Its high melting temperature, high thermal conductivity, low sputtering yield, and low tritium retention enable its applicability in the extremely hostile fusion environment, characterized by high temperature, and high fluxes of heat (i.e., >10 $MW/m^2$) and particles (i.e., D, T, He, and neutrons). The combined effect of these loading conditions imposes significant challenges to W performance in service. One of the primary concerns is the significant displacement damage of lattice structure creating vacancies, interstitials, and their clusters, as well as generating significant concentrations of transmutation elements (i.e., Re, Os), induced by the 14 MeV-peak fusion neutron spectra. Under first wall power-plant conditions, calculations showed that Re converted from W reaches a concentration of 3.8 at% after five years from (n, β) nuclear reactions, with Os at a slightly lower level of 1.4 at% [1].

Irradiation effects in W have drawn a great deal of attention in response to its application as plasma facing material. However, due to the lack of fusion-relevant neutron sources, the investigation of neutron irradiation effects of W has been centered on the use of fission neutron reactors and accelerator-based ion beams serving as surrogates for neutron irradiation. Microstructure characterization of neutron-irradiated tungsten [2] [3] indicates that a high number density of prismatic dislocation loops are the

dominant defect features in the low irradiation dose region, up to 0.15 dpa [3-6]; a void lattice develops at irradiation dose of ~ 1 dpa; when irradiation dose is greater than 5 dpa for fast neutron irradiation or 1.4 dpa in mixed energy spectrum reactors, a high density of precipitates with acicular shape emerge at Re concentrations well below the solubility limit [4, 7]. Self-ion irradiations of W and W-alloys were also extensively studied to characterize the irradiation defects and mimic the transmutation precipitation behavior [8-10]. The unique defect feature, transmutation induced precipitates, complicates the microstructural evolution and leads to an abnormal irradiation hardening behavior of neutron-irradiated W [11] [7] [12] [13] [14] [15]. The measured hardness continuously increases exponentially in contrast to the irradiation hardening behavior of other metals, where hardness reaches saturation at some certain irradiation dose [15].

Although many aspects of the irradiation effects in W have been revealed, the highly interrelated phenomena of transmutant elements-defect interactions and the precipitation are not sufficiently understood. In particular, the detailed characterization of the precipitates and the dynamic process of precipitation in neutron-irradiated W are less explored. Early studies before 2000 on transmutation induced precipitation phenomena used neutron-irradiated W-Re alloys with the motivation of understanding irradiation induced solute segregation and precipitation. Sikka and Moteff [16] identified the α-Mn crystal structure (i.e., χ phase, $WRe_3$) of the precipitates in W-25%Re alloys subjected to fast neutron irradiation to a fluence of ~$1\times10^{22}$ n/cm$^2$ (E > 1MeV) in the temperature range of 430~1000°C by combining the electron diffraction pattern with the W-Re phase diagram. Williams et al. [17] investigated W-based alloys containing 5%, 11%, and 25% Re irradiated in the Experimental Breeder Reactor (EBR-II) to a fluence of $6\times10^{21}$ n/cm$^2$

(E > 0.1 MeV) at 900~1500°C and found the precipitates in all samples. They also identified the precipitates as cubic, Re-rich χ phase and observed large variations in precipitate morphology and distribution. Herschitz and Seidman [18] [19] performed further investigations of W-10%Re and W-25%Re alloys irradiated in EBR-II at 575, 625 and 675°C to 8.6 dpa using the atom-probe field-ion microscope. Homogeneous Re-rich χ phase precipitation were also found without association with other defects or impurity atoms. Driven by the need to develop plasma facing material for fusion reactors, the binary W-Re alloys have been proposed to increase the recrystallization temperature and ductility [20] in response to the undesired embrittlement of pure W. Nemoto et al. [21] used TEM dark field imaging to characterize the microstructure of W-26%Re exposed to neutron irradiation in the Fast Flux Test Facility to a dose range of 2~11 dpa at 373~800 °C. Their results showed the presence and morphology of both σ and χ phase precipitates with equiaxed and lenticular morphology, respectively. A research group at Tohoku University carried out extensive microstructure characterization of W and W-alloys irradiated in various fission reactors (i.e., a sodium-cooled fast reactor JOYO; the Japan Material Testing Reactor – JMTR; the High Flux Isotope Reactor – HFIR, USA) using TEM. He et al. [22] found the formation of precipitates at grain boundaries in W-26%Re irradiated at 800°C to 0.15 dpa in JMTR. Tanno et al. [23] showed the σ and χ phase precipitates were observed in W-5%Re and W-10%Re alloys irradiated in JOYO at 400~750°C to 1.54 dpa. Fukuda et al. [3] observed large amounts of precipitates identified as σ and χ phase in all W-Re alloys irradiated in HFIR at 500 and 800°C to 1 dpa. However, these studies were based on neutron-irradiated W-Re alloys and thus only provided limited insights into the transmutation induced precipitation in W, without

capturing the mutual interactions of irradiation induced defects and the transmutant Re and Os in the early stage as well as the corresponding kinetics process.

The transmutation induced precipitates in high purity W were studied to some limited extent. In Ref. [3], σ and χ phase precipitates were identified in W irradiated at 500 and 800°C to ~1 dpa in HFIR, using the same method shown in [21]. Koyanagi et al. [4] found Re- and Os-rich precipitates along grain boundaries in polycrystalline W following neutron irradiation at 650°C to 2.4 dpa and at 500°C to 4.6 dpa in HFIR. Hwang et al. [24] characterized the Re-enriched clusters in pure tungsten irradiated in HFIR to 0.9 dpa at 500°C by using atom probe tomography and TEM. In addition, several theoretical studies are available to assist the understanding of transmutation-induced precipitation. Density Functional Theory (DFT) calculations [25] [26] [27] have been performed to investigate the energetics of Re and Os in tungsten. Kinetic Monte Carlo simulations [28] were employed to explore the mechanisms of nucleation and growth of Re clusters in irradiated W-Re alloys.

Despite a wealth of experimental work as well as limited theoretical work performed to investigate the transmutation-induced precipitation in neutron-irradiated tungsten and its alloys, knowledge gap still exists in the detailed characterization of precipitates (e.g., compositions, phases, crystalline structures, preferential orientations, etc.) and the kinetic process of the precipitation in neuron-irradiated pure tungsten (i.e., the incipient clustering of transmutant elements and the subsequent growth leading to the formation of precipitates). In this study, microstructure characterization of tungsten irradiated to various conditions is presented to show the kinetics process of transmutation-induced precipitation. The corresponding underlying mechanisms

controlling the precipitation process are discussed based on the available fundamentals of the interactions between transmutant elements and intrinsic radiation defects.

## 2. Experiment

High purity single crystal W specimens (nominal 99.999%, oriented along [110]) were purchased from Goodfellow, USA. The major impurities are 10 ppm O, <10 ppm N, 20 ppm C, <5 ppm S, 3 ppm H, and 140 ppm Cu. The polycrystalline W specimens ($16\times4\times0.1$ mm$^3$) used in this study were provided by Plansee, Austria produced by powder sintering and then hot and cold rolling with a purity of 99.97% (<100 ppm Mo, <30 ppm C, <30 ppm Fe, and < 20ppm O, guaranteed by the manufacturer). Electron Backscatter Diffraction (EBSD) analysis of the W foil surface indicated that the average grain size was ~ 5 μm. The majority of the grains elongated to <1 0 1> axis, corresponding to the rolling direction and low angle grain boundaries were dominant [4].

Neutron irradiation was performed in the HFIR at Oak Ridge National Laboratory (ORNL). The irradiation conditions of the samples studied are listed in Table 1. In HFIR, a neutron fluence of $1 \times 10^{25}$ n/m$^2$ (E > 0.1 MeV) corresponds to 0.2 displacements per atom (dpa) in tungsten with a rate of $2.3\times10^{-7}$ dpa/s. The concentrations of transmutant elements were calculated using FISPACT-II [29]. The actual irradiation temperatures of the neutron-irradiated samples were determined based on annealing behavior of a passive SiC temperature monitor placed in the sample irradiation capsule during continuous dilatometry [30]. The uncertainty of temperature determination was ±10°C.

Microstructure characterization was carried out in the low activation materials development and analysis (LAMDA) laboratory [31] at ORNL. Electron transparent TEM foils were prepared using a focus ion beam system (FEI Quanta 3D Dual Beam)

operated at 30 kV for initial milling and at 5 kV for final thinning to minimize any FIB-induced damages. The lifted-out foils also underwent an additional 900 eV Ar ion milling using a Fischione Model 1040 NanoMill to further thin and clean the foils prior to the microstructural investigations. TEM examination was performed in a FEI Talos F200X S/TEM (200 keV, Schottky-emission, non-aberration-corrected) equipped with a SuperX four-detector X-ray energy dispersive spectroscopy (EDS) system. EDS mapping used a small condenser aperture (convergence semiangle ~8 mrad) to minimize beam spread in the thin foils.

## 3. Results

### 3.1 General microstructure of tungsten following neutron irradiation

As shown in [32], positron annihilation lifetime spectroscopy measurements confirmed the existence of small vacancy clusters in as-received single crystal tungsten, while no visible dislocation loops or line dislocations were observed in the same sample via TEM observations. The as-received polycrystalline W samples contain a high number density of line dislocations stemming from the hot rolling process [4]. Dislocations, voids, and precipitates are three common defect features found in neutron-irradiated tungsten, which are strongly dependent on the irradiation temperature, dose, and neutron energy spectrum. Figure 1 shows representative TEM images of the typical defect features in two selected samples. Voids, dislocation loops and line dislocations were observed in all the samples in the present study. Acicular precipitates were found in the single crystal tungsten irradiated to 0.6 dpa at 1100°C and to 1.80 dpa at 770°C as well as in the two polycrystalline tungsten samples irradiated to a dose of > 1.5 dpa at 800°C. In

order to avoid repetition, general TEM analysis of the microstructures of neutron-irradiated W will not be introduced here. More details can be found in Ref. [4].

### 3.2 Characterization of transmutation-induced precipitates in neutron-irradiated tungsten

Figure 2 shows the STEM dark field images and X-ray maps of single crystal tungsten with an orientation of (110) following neutron irradiation. The size and number density of the observed W-Re-Os clusters/precipitates are summarized in Table 2. In Ref. [4], X-ray maps of polycrystalline tungsten samples with irradiation dose higher than 2 dpa were shown. The conventional JEOL JEM2100F EDS employed could only resolve the chemical information of the large precipitates enriched in Re and Os along grain boundaries, while the chemical analysis of the small W-Re-Os clusters/acicular precipitates within the grains was not available. In the current study, the use of the FEI Talos F200X S/TEM equipped with SuperX four-detector energy dispersive X-ray spectroscopy enabled the X-ray mapping with much better resolution. In the present study, the nanoscale clusters are those features enriched in Re and Os, shown in X-ray map, but showing no obvious diffraction contrast in TEM or STEM imaging. Therefore, we infer the clusters are likely areas of solute enrichment or segregation in the native host BCC structure. The acicular precipitates are defined as the needle-shape microstructure features having the strong diffraction contrast compared to matrix in HAADF images.

The X-ray maps indicate that the configuration and concentration of transmutant elements are functions of irradiation dose and temperature. Generally, when irradiation dose is less than 0.44 dpa, nanoscale W-Re-Os clusters are observed. Acicular precipitates enriched in Re and Os are formed in the sample irradiated to 1.80 dpa at

770°C. In 1W47 (0.02 dpa, 460°C), dislocations are predominant defect features. Although the transmutation in this low dose sample is in a low level (0.28% Re and 0.013% Os), nanoscale W-Re-Os clusters are already visible. Due to the low concentration, Os clusters are not obvious. Dislocations are found in the same positions as visible W and Re enriched clusters shown in Figure 2(a). Note that not all dislocations shown in the DF image have the enriched Re and Os. In the sample irradiated to 0.09 dpa at 797°C, Figure 2(b), nanoscale W-Re-Os clusters with sparse distribution are found with more concentrated Re and Os in comparison with the sample irradiated to 0.02dpa. The tungsten sample irradiated at 705°C to 0.44 dpa has a relative homogenous distribution of larger W-Re-Os clusters, Figure 2(c). The average size and number density of nanoscale clusters increase with increasing irradiation dose, as shown in Table 2. A much more complicated microstructure characterized by the coexistence of a large number of voids and acicular precipitates enriched in Re and Os is developed in the single crystal tungsten sample irradiated to 1.80 dpa at 770°C. However, the exact threshold of irradiation dose allowing the formation of acicular precipitate can not be obtained due to lack of experimental data in the range from 0.44 to 1.8 dpa in the present study.

Figure 3 shows the high angle annular dark field (HAADF) images and X-ray maps of polycrystalline tungsten irradiated to two different conditions. Voids and precipitates are predominant defect features within the grains. A high number density of voids are homogenously distributed throughout the gains in both samples. The average sizes of voids in OW158 (1.5 dpa, 800°C, Figure 3(a)) and OW125 (2.4 dpa, 800°C, Figure 3(b)) are 5.6 and 5.8 nm, respectively, while the corresponding number densities

are $4\times10^{21}$ and $6\times10^{21}$ $m^3$, respectively. The dense acicular precipitates disperse within grains while large plate-shape precipitates are formed along grain boundaries or in the intersection of grain boundaries. The average number densities of acicular precipitates within the grains of OW158 and OW125 are $5\times10^{21}$ and $1.0\times10^{22}$ $m^3$, respectively, and the average lengths are 24.7 and 30.5 nm, respectively. In addition, strong affiliations of precipitates with voids are observed from these 2-D TEM images, although further evidence is needed to confirm their association. A narrow denuded zone with a width of ~20 nm along grain boundaries exists in the observed areas. X-ray maps show a relatively homogeneous distribution of precipitates dispersed within the grains. It is found that Os is evidently found in the large precipitates with very limited additional segregation to the grain boundaries while Re was not only present in the precipitates but also accumulated along the grain boundary. It is likely that the Os contained in the large precipitates were mainly formed by the nuclear reaction of the Re atoms which are already clustered, not the segregation of Os atoms diffusing from the grains.

TEM images at higher magnification shown in Figure 4 provide more details of the interaction between voids and precipitates in a local zone near a grain boundary of OW158 (1.5dpa, 800°C). It is apparent that all visible voids are embedded in the acicular Re-Os-rich precipitates. In contrast, not all observed precipitates are bonded to voids. Some of the visible voids were partially intersected by the associated precipitates while some are completely surrounded by the precipitates. Both faceted and round voids exist. The same correlation of voids and precipitates is also observed in OW125 (2.4dpa, 800°C) and 1W19 (1.8dpa, 770°C). In all previous studies, the transmutation-induced precipitates in neutron-irradiated tungsten were defined as either $\sigma$ or $\chi$ phases based on

the W-Re or W-Os phase diagram. A reassessment of the precipitates phases in neutron-irradiated tungsten together with the orientations and quantitative information is being performed in our group and the results will be available elsewhere.

When comparing the microstructure of the single crystal and polycrystalline tungsten following neutron irradiation, it is found that the defect features contained within the grains in the polycrystalline sample are similar to those of single crystal tungsten with similar irradiation conditions, consisting of dense acicular precipitates and voids. The grain boundaries in polycrystalline tungsten act as strong defect sinks, resulting in segregation of transmutant elements and the formation of large precipitates along grain boundaries. In single crystal tungsten, the lack of the grain boundaries ensures that all transmutant elements as well as the radiation damage is involved in the defect evolution within the grains. Therefore, it is deduced that the number density and size of precipitates in single crystal tungsten are larger than those in the grains of polycrystalline tungsten following identical irradiation conditions, ignoring the difference in impurities.

## 4. Discussion

### 4.1 Association of voids and precipitates/transmutant elements clusters

Strong affiliation of voids and precipitates were observed in both single and poly-crystalline tungsten, as shown in Figures 2(d), 3, and 4. However, it is not possible to determine whether the voids and precipitates are associated or not based only on the 2-D TEM images. In order to address this question, a local area with a thickness of ~ 50 nm in OW158 was tilted by ±20° with respect to X-axis. STEM bright field images of this area at 2 different tilt positions are shown in Figure 5(a). If the voids and precipitates are not

associated with each other and the apparent association in the 2D TEM images arose from the overlap of the two defect features in the TEM foil depth direction with a gap between them, the relative positions of these two features will be changed when tilting the samples. Assuming the distance in depth direction of one void and one precipitate is 35 nm, the maximum 20° tilt gives rise to a 12 nm separation. However, the relative positions of voids and precipitates in the observed regions barely changed. Therefore, the visible voids and precipitates in the neutron-irradiated tungsten are strongly associated with each other. In order to better demonstrate the relative positions of voids and precipitates, three dimensional images of precipitates/voids were obtained using a tomographic model based on stereomicroscopy, which treats features as discrete points or series of points in space [33] [34]. The precipitates were treated as straight lines between discreet points at each end of a precipitate. Cavities were treated as spheres. A similar approach is detailed in Ref. [35]. Visualization of the models was performed using Mayavi [36]. Figure 5(b) shows the overlapping of model generated precipitates and voids with TEM images. Snapshots of the movies showing the relative positions of precipitates and voids in a 3D modeling box are presented in Figure 5(c). The movie is available in the supplementary materials.

One interesting question is which is formed first, void or precipitate. TEM observation of tungsten irradiated at 460°C to 0.02dpa showed the existence of voids [4]. As discussed in Section 3.2, very limited amount of Re (0.28%) and Os (0.01%) were generated in this sample. Only nanoscale W-Re-Os clusters with very low number density were formed. Therefore, the formation of acicular precipitates is preceded by voids. The formation of visible voids in such low dose and low temperature seems to be

surprising since the migration energy of vacancy in tungsten is high, in the range 1.29 eV to 2.34 eV [37]. In contrast, the isochronal annealing study of tungsten irradiated at 90°C to 0.03dpa showed vacancy mobility was already observed at 400°C [32]. Figure 6 shows the defect cluster production rate in tungsten exposed to HFIR neutrons, which was calculated by incorporating the defect production database from MD simulations [38] and the neutron energy spectrum of the flux trap facility. It is apparent that very large vacancy clusters in 3-D shape containing more than 80 vacancies, equivalent to a nano-void with a diameter of 1.3 nm, could be directly formed from displacement cascades. This could also explain the existence of visible voids in the low dose tungsten samples. In addition, large dislocation loops (>3.4 nm) could also be directly produced from the displacement cascades.

**4.2 Comparison of precipitates in ion/neutron-irradiated W-alloys and neutron-irradiated W**

Solute atom clustering and precipitation in ion or neutron-irradiated tungsten alloys have been studied by numerous research group. For example, Xu et al. [39] [10] investigated the ion-irradiation-induced clustering in W-Re and W-Re-Os alloys using atom probe tomography (APT). Their results showed that W-Re clusters with radius of 2.39 and 3.3nm were found in W-2 at.%Re alloy irradiated by 2 MeV tungsten ions to a fluence of $2.64\times10^{15}/cm^2$ (equivalent to a peak damage level of 33 dpa) at 300°C and 500°C, respectively. Similarly, only small W-Re-Os clusters could be found in the W-1at.%Re-1at.%Os irradiated under the same conditions. These results are similar to the W-Re-Os clusters observed in the low dose neutron-irradiated tungsten, Figure 2 (a), (b) and (c), but much smaller. No acicular precipitates were found in the ion irradiation

studies of tungsten alloys available in the literature. Tanno et al. [40] [23] identified the χ phase acicular precipitates in W-5at%Re, W-5at%Os, and W-5%atRe-3%atOs irradiated in JOYO, a fast reactor, at 750°C to 1.54 dpa. The fast neutron spectrum resulted in only limited formation of transmutant elements during the irradiation. The pre-existing Re and Os serves as the source for the subsequent precipitation.

Due to the large energy transfer cross section of ion irradiation, the irradiation damage is strongly localized. The peak damage areas have more significant microstructural evolution in terms of the production of vacancy and interstitial clusters, migration of solute atoms, etc. The absence of large W-solute clusters or precipitates implies that the local concentration of Re (2% in their studies) is not sufficient to provide the source for precipitates through the migration of W-Re dumbbells in the ion irradiation study. In addition, the relatively lower irradiation temperatures (300 and 500°C) also lead to the lower mobility of mobile species in comparison with the neutron irradiation conditions. This is evident in the light of the APT analysis that the average Re concentration in the clusters is only 6.5% [39] [10]. Therefore, the clustering of these elements is much less profound in comparison with that of neutron-irradiated tungsten, implying that the neutron irradiation induced more dramatical interactions between the transmutant elements and the radiation defects through radiation-enhanced diffusion and the overlap of displacement cascades, which induced the formation of precipitates.

A noticeable feature of the clustering or precipitation observed in the ion or neutron-irradiated tungsten alloys is that the elements involving in the process of clustering/precipitation existed in the initial state and their total amount stayed constant (or approximately constant for the fast neutron irradiated alloys) during this non-

equilibrium process under irradiation. However, in the present study and in the practical application environment, the starting material is high purity tungsten. With increasing irradiation dose, tungsten atoms were gradually converted to Re and Os by nuclear reaction, leading to the formation of a ternary alloy with evolving composition. The interactions between intrinsic radiation defects and the gradually-generated transmutant elements give rise to the segregation and precipitation.

**4.3 Mechanisms controlling transmutation induced precipitation in tungsten**

Figure 2 can be used as a rough roadmap of the kinetic process of transmutation-induced precipitation in neutron-irradiated tungsten, even though the irradiation temperatures are not constant. Nanoscale segregation of W-Re-Os was observed within the sample irradiated to a dose as low as 0.02 dpa when very limited transmutant elements were present. Os, a secondary transmutant element from tungsten, started to be involved in the segregation with increasing irradiation dose. With irradiation dose continuously increasing, more transnutant elements were produced as well as more radiation damage, resulting in a relatively homogeneous distribution of W-Re-Os clusters, which acted as nucleation sites for further precipitation. In the 1.80 dpa sample, the continuous clustering of transmutant elements and defects leads to the formation of dense acicular W-Re-Os precipitates, which were also observed in the two polycrystalline tungsten irradiated to 1.5 and 2.4 dpa, respectively. A data gap between 0.44 and 1.5 dpa still exist, in which a transition process from W-Re-Os clusters to acicular precipitates is expected.

The precipitates were observed in neutron-irradiated tungsten with transmutant Re and Os concentration well below the solubility limit. Actually, precipitation of non-

equilibrium phases in irradiated binary or more complex alloys is commonplace. The standard theory of irradiation damage includes radiation-enhanced diffusion and radiation-induced precipitation as mechanisms that can drive the system out of equilibrium due to the onset of point defect cluster fluxes towards defect sinks, known as inverse Kirkendall effects [28]. In tungsten, the transmutation complicates the process by introducing a material system with evolving compositions. Understanding the underlying mechanisms controlling the precipitation relies on knowing the fundamentals of the interactions between irradiation induced defects and transmutant elements. DFT simulations [25, 26] showed that solute Re and Os atoms are both attracted to tungsten self-interstitials (SIAs) with binding energies of 0.79 and 1.87 eV, respectively. In contrast, the trapping of solute transmutant elements in vacancy defects is relatively weak since the binding energies of Re and Os to vacancy are 0.22 and 0.53eV, respectively. Due to the larger binding energy of SIA-Re/Os, the large interaction range, and the extremely high mobility, SIA will be preferentially trapped by solute Re and Os rather than recombining with vacancies. SIAs migrate along <111> direction until they encounter solute atoms, after which a mixed W-Re or W-Os dumbbell is formed. The low rotation barrier (0.03eV) and the high binding energy (0.79 eV) enable 3D motion of W-Re dumbbells with a rotation path of <111> ➔ <110>➔<111>. A similar migration behavior is also expected for W-Os dumbbells with relatively higher rotation barrier of 0.16eV and different rotation path of <110> ➔ <111>➔<110>. Huang et al. [28] carried out kinetic Monte Carlo simulation of Re cluster formation in irradiated W-2%Re alloys and found that mixed-interstitial solute transport control cluster nucleation and growth. Vacancies serve a dual purpose. First, they act as a ‘hinge’ between solute atoms that

would otherwise repel, resulting in an initial positive contribution by forming small solute clusters. Once a critical nucleus forms and starts to grow, vacancies act to dissolve the precipitates by making the precipitates/matrix interface more diffuse. Sustained capture of mixed interstitials and vacancies give rise to the localized recombination at the precipitates and segregation of solute atoms over time, leading to the accumulation of transmutant elements in the vicinity of voids. This also rationalized the observed strong association of voids and precipitates, as shown in Section 4.1. The first-principles calculation done by Li et al. [27] indicated that $Re_x$-SIA and $Os_x$-SIA clusters are very stable and the binding energies increase with increasing Re/Os atom numbers contained within the clusters. Os-contained clusters are more stable in comparison with Re-contained clusters. Therefore, it is believed that the formation of the observed W-Re-Os clusters shown in Fig. 2 (a), (b) and (c) resulted from this interstitial-mediated segregation process. These clusters will further act as trapping centers for subsequent aggregation of mobile W-Re/Os dumbbells, vacancies and SIAs. However, the formation mechanism of the acicular-shape precipitates along <111> direction is unknown at this moment. A postulated theory is that growth of precipitates along <111> is energetically preferred. More theoretical work is needed to investigate the energetics of large W-Re-Os precipitates with respect to the preferred orientation and configurations.

Defect features (e.g, dislocations and voids) contained in the neutron-irradiated tungsten act as potential nucleation sites for the transmutation-induced precipitates. As shown in Figure 2(a), Re and Os clusters were found in the same positions as dislocations in the sample irradiated to 0.02 dpa at 460°C. The high mobility of W-Re/Os dumbbells resulted in the segregation of Re and Os in the dislocations. This process is more

significant in the low dose tungsten samples, where dislocations are predominant defects. The voids formed in the early stage of irradiation are also expected to act as nucleation sites for transmutant element clusters, promoting the subsequent growth of precipitates. X-ray maps of 1W17 (0.44 dpa, 707°C) showing the correlation of voids and transmutant elements clusters provided direct evidence for this mechanism. As shown in Figure 7, HAADF micrograph showed the existence of a large number density of voids in 1W17. X-ray maps overlapped with HAADF image are also shown. It is apparent that Re and Os segregate around voids, implying voids are trapping sites for transmutant elements. These Re/Os cluster-void complexes are the precursors of the observed assembly of acicular precipitates and voids shown in Figures 2(d), 3 and 4. It also rationalized the observation that all visible voids were embedded in the acicular precipitates in W following high dose irradiation (>1.5dpa). The fact that not all acicular precipitates are embracing voids, discussed in Section 3.2, indicates that other nucleation sites are present in addition to voids, likely dislocations.

**4.4 Thermal stability of the W-Re-Os clusters**

As a fusion reactor plasma facing material, tungsten is subject to very high thermal flux (>10 MW/m$^2$) and high temperature in addition to the neutron irradiation and ion bombardment. Under normal operation, the temperatures of tungsten plasma facing components are in a range 550 to1450°C, depending on the positions and the coolant [41]. The recommended maximum operation temperature of tungsten should be less than its recrystallization temperature, which ranges from 1100 to 1300 °C depending on the thermal annealing duration [42]. Lower annealing temperatures require longer durations to achieve recrystallization of tungsten [42]. It is unknown whether precipitates

will be formed in tungsten in such high temperature environments. The thermal stability of W-Re-Os clusters will help to address this question. There is apparently no available theoretical analysis of the energetics of W-Re-Os clusters. The thermal stability of this ternary cluster was assessed by characterizing the tungsten sample irradiated in HFIR at 705°C to 0.44 dpa followed by a thermal annealing at 1200°C (ramp rate of 0.5°C/s) for 2 hours in an ultra-high vacuum ($2\times10^{-8}$ torr). A homogeneous distribution of W-Re-Os clusters was found in the as-irradiated state, shown in Fig. 8 (a). Figure 8 (b) refers to the X-ray maps of the same sample following 2-h anneal at 1200°C. It is apparent that the ternary W-Re-Os clusters are dissolving in the matrix following the 1200°C anneal. Therefore, 1200°C is sufficiently high to drive the dissociation of W-Re-Os alloys. The high mobility of vacancy at this temperature also induces sufficient solute transport leading to the dissolution of these clusters. In the practical application environment, the continuous production of irradiation damages and transmutant elements is expected to alter the thermodynamics of W-Re-Os clusters and promotes the further nucleation and growth of transmutation-induced precipitates. In a recent neutron irradiation campaign on tungsten, a single crystal tungsten sample with orientation of (110), SX55, was irradiated at 1100°C to 0.6 dpa in the same reactor. X-ray maps, Figure 9, showed the formation of acicular precipitates enriched in Re and Os with very sparse distribution, providing direct evidence of the high temperature stability of precipitates in tungsten exposed to neutron irradiation. However, APT analysis [24] of tungsten sample irradiated at 500°C to 0.9 dpa in HFIR indicated that only nanoscale clusters were found. The high irradiation temperature resulted in extemely high mobility of involving species, promoting the formation of acicular precipitates in lower irradiation dose samples. Apparently,

irradiation temperature determining the thermal mobility of defect features is also a critical parameter impacting the transmutation-induced precipitation in addition to the irradiation dose. As shown in Figure 9, it is found that transmutant Os is more concentrated while Re is more dissolved in the sample irradiated at 1100°C to 0.6 dpa. Some of the visible precipitates are only enriched in Os while the segregation of Re around the precipitates is not obvious. This is consistent with the theoretical analysis that Os-contained clusters are more stable in comparison with Re-contained clusters [27].

**5. Conclusion**

Defect features consisting of transmutant elements in tungsten irradiated at 460~1100°C to 0.02~2.4dpa in HFIR were characterized using TEM. The general process of transmutation-induced precipitation was revealed by capturing the microstructures of tungsten irradiated to various conditions. The main results are summarized as follows:

(1) The configuration and size distribution of defect features consisting of Re and Os in neutron-irradiated tungsten are strongly dependent on the irradiation dose and temperature. Nanoscale clusters enriched in Re and Os were observed in the low dose regime from 0.02 to 0.44 dpa while acicular-shape precipitates appeared when irradiation dose is higher than 1.8 dpa in single crystal tungsten irradiated in the temperature regime 460°C to 770°C.

(2) Large plate-shape precipitates were found along grain boundaries or in the intersection of grain boundaries in neutron-irradiated polycrystalline tungsten. The intragranular precipitates are similar to those found in single crystal tungsten.

(3) A rough roadmap of the kinetics process of the transmutation-induced precipitation in neutron-irradiated tungsten was presented. Nanoscale segregation of W-Re-Os was observed within the sample irradiated to a dose as low as 0.02 dpa. With irradiation dose continuously increasing, more transnutant elements were produced as well as more radiation damage, resulting in a relatively homogeneous distribution of W-Re-Os clusters, which acted as nucleation sites for further precipitation. In the 1.80 dpa sample, the continuous clustering of transmutant elements and defects leads to the formation of dense acicular W-Re-Os precipitates, which were also observed in the two polycrystalline tungsten irradiated to 1.5 and 2.4 dpa, respectively. A data gap between 0.44 and 1.5 dpa still exist, in which a transition process from W-Re-Os clusters to acicular precipitates is expected. The segregation and precipitation are controlled by the highly mobile W-Re and W-Os dumbbells.

(4) All TEM-visible voids were associated with the acicular-shape precipitates. Voids were formed prior to the formation of acicular-shape precipitates based on the series of TEM observations and are expected to act as strong trapping sites for mobile species involving in the precipitation to promote the nucleation and growth of precipitates. In addition, dislocations are also nucleation sites.

(5) Os is more concentrated in both W-Re-Os clusters (Os found in the center of the clusters) and precipitates (sharper boundaries as observed in the EDS analysis) in comparison with the Re.

(6) 2-h anneal at 1200°C of tungsten irradiated to 0.44 dpa at 705°C leads to the dissociation of the nanoscale W-Re-Os clusters. However, acicular precipitates were found in tungsten irradiated at 1100°C to 0.6 dpa.

## Acknowledgement

This work was partially supported by Laboratory Directed R&D funds at ORNL. The research was also sponsored by the US Department of Energy Office of Fusion Energy Science under grant DE-AC05-00OR22725 with UT-Battelle LLC. Strong supports from HFIR and LAMDA staff are greatly appreciated. This work was partly performed at Los Alamos National Laboratory supported by funding from DOE-NE's Nuclear Technology Research and Development program. Los Alamos National Laboratory, an affirmative action equal opportunity employer, is operated by Los Alamos National Security, LLC, for the National Nuclear Security Administration of the U.S. Department of Energy under contract DE-AC52-06NA25396.

## References

[1] M.R. Gilbert and J.C. Sublet, Neutron-induced transmutation effects in W and W-alloys in a fusion environment, Nucl. Fusion 51 (2011) 043005.
[2] A. Hasegawa, M. Fukuda, T. Tanno, and S. Nogami, Neutron irradiation behavior of tungsten, Mater. Trans. 54 (2013) 466–471.
[3] M. Fukuda, K. Yabuuchi, S. Nogami, A. Hasegawa, and T. Tanaka, Microstructural development of tungsten and tungsten-rhenium alloys due to neutron irradiation in HFIR, J. Nucl. Mater. 455 (2014) 460–463.
[4] T. Koyanagi, N.A.P.K. Kumar, T. Hwang, L.M. Garrison, X. Hu, L.L. Snead, and Y. Katoh, Microstructural evolution of pure tungsten neutron irradiated with a mixed energy spectrum, J. Nucl. Mater. 490 (2017) 66–74.
[5] M. Fukuda, N.A.P. Kiran Kumar, T. Koyanagi, L.M. Garrison, L.L. Snead, Y. Katoh, and A. Hasegawa, Neutron energy spectrum influence on irradiation hardening and microstructural development of tungsten, J. Nucl. Mater. 479 (2016) 249–254.
[6] A. Hasegawa, M. Fukuda, S. Nogami, and K. Yabuuchi, Neutron irradiation effects on tungsten materials, Fusion Eng. Des. 89 (2014) 1568–1572.
[7] A. Hasegawa, T. Tanno, S. Nogami, and M. Satou, Property change mechanism in tungsten under neutron irradiation in various reactors, J. Nucl. Mater. 417 (2011) 491–494.
[8] X. Yi, M.L. Jenkins, K. Hattar, P.D. Edmondson, and S.G. Roberts, Characterisation of radiation damage in W and W-based alloys from 2MeV self-ion near-bulk implantations, Acta Mater. 92 (2015) 163–177.
[9] F. Ferroni, X. Yi, K. Arakawa, S.P. Fitzgerald, P.D. Edmondson, and S.G. Roberts, High temperature annealing of ion irradiated tungsten, Acta Mater. 90 (2015) 380–393.

[10] A. Xu, C. Beck, D.E.J. Armstrong, K. Rajan, G.D.W. Smith, P.A.J. Bagot, and S.G. Roberts, Ion-irradiation-induced clustering in W-Re and W-Re-Os alloys: A comparative study using atom probe tomography and nanoindentation measurements, Acta Mater. 87 (2015) 121–127.
[11] T. Tanno, A. Hasegawa, J.-C. He, M. Fujiwara, S. Nogami, M. Satou, T. Shishido, and K. Abe, Effects of Transmutation Elements on Neutron Irradiation Hardening of Tungsten, Mater. Trans. 48 (2007) 2399–2402.
[12] M. Fukuda, A. Hasegawa, T. Tanno, S. Nogami, and H. Kurishita, Property change of advanced tungsten alloys due to neutron irradiation, J. Nucl. Mater. 442 (2013) S273–S276.
[13] M. Fukuda, T. Tanno, S. Nogami, and A. Hasegawa, Effects of Re Content and Fabrication Process on Microstructural Changes and Hardening in Neutron Irradiated Tungsten, Mater. Trans. 53 (2012) 2145–2150.
[14] M. Fukuda, N.A.P. Kiran Kumar, T. Koyanagi, L.M. Garrison, L.L. Snead, Y. Katoh, and A. Hasegawa, Neutron energy spectrum influence on irradiation hardening and microstructrual development of tungsten, J. Nucl. Mater. 479 (2016) 249–254.
[15] X. Hu, T. Koyanagi, M. Fukuda, N.A.P.K. Kumar, L.L. Snead, B.D. Wirth, and Y. Katoh, Irradiation hardening of pure tungsten exposed to neutron irradiation, J. Nucl. Mater. 480 (2016) 235–243.
[16] V.K. Sikka and J. Moteff, Identification of alpha-Mn crystal structure in neutron irradiated W-Re alloy, Metall. Trans. 5 (1974) 1514–1517.
[17] R.K. Williams, F.W. Wiffen, J. Bentley, and J.O. Stiegler, Irradiation induced precipitation in tungsten based, W-Re alloys, Metall. Mater. Trans. A 14 (1983) 655–666.
[18] R. Herschitz and D.N. Seidman, An atomic resolution study of homogeneous radiation-induced precipitation in a neutron irradiated W-10at.% Re alloy, Acta Metall. 32 (1984) 1141–1154.
[19] R. Herschitz and D.N. Seidman, An atomic resolution study of radiation-induced precipitation and solute segregation effects in a neutron-irradiated W-25 at.% Re alloy, Acta Metall. 32 (1984) 1155–1171.
[20] P. Makarov and K. Povarova, Development of tungsten-based vacuum melted and powder structural alloys, Int. J. Refract. Met. H. 20 (2002) 277–285.
[21] Y. Nemoto, A. Hasegawa, M. Satou, and K. Abe, Microstructural development of neutron irradiated W-Re alloys, J. Nucl. Mater. 283–287 (2000) 1144–1147.
[22] J.C. He, G.Y. Tang, A. Hasegawa, and K. Abe, Microstructural development and irradiation hardening of W and W-(3-26) wt%Re alloys after high–temperature neutron irradiation to 0.15 dpa, Nucl. Fusion 46 (2006) 877–883.
[23] T. Tanno, M. Fukuda, S. Nogami, and A. Hasegawa, Microstructure Development in Neutron Irradiated Tungsten Alloys, Mater. Trans. 52 (2011) 1447–1451.
[24] T. Hwang, A. Hasegawa, K. Tomura, N. Ebisawa, T. Toyama, Y. Nagai, M. Fukuda, T. Miyazawa, T. Tanaka, and S. Nogami, Effect of neutron irradiation on rhenium cluster formation in tungsten and tungsten-rhenium alloys, J. Nucl. Mater. 507 (2018) 78–86.
[25] T. Suzudo, M. Yamaguchi, and A. Hasegawa, Stability and mobility of rhenium and osmium in tungsten: first principles study, Model. Simul. Mater. Sci. Eng. 22 (2014) 075006.

[26] T. Suzudo, M. Yamaguchi, and A. Hasegawa, Migration of rhenium and osmium interstitials in tungsten, J. Nucl. Mater. 467 (2015) 418–423.
[27] Y.-H. Li, H.-B. Zhou, H. Deng, G. Lu, and G.-H. Lu, Towards understanding the mechanism of rhenium and osmium precipitation in tungsten and its implication for tungsten–based alloys, J. Nucl. Mater. 505 (2018) 30–43.
[28] C.-H. Huang, L. Gharaee, Y. Zhao, P. Erhart, and J. Marian, Mechanism of nucleation and incipient growth of Re clusters in irradiated W-Re alloys from kinetic Monte Carlo simulations, Phys. Rev. B 96 (2017)
[29] http://fispact.ukaea.uk.
[30] A.A. Campbell, W.D. Porter, Y. Katoh, and L.L. Snead, Method for analyzing passive silicon carbide thermometry with a continuous dilatometer to determine irradiation temperature, Nucl. Instr. Meth. Phys. Res. B 370 (2016) 49–58.
[31] C.M. Parish, N.A.P. Kiran Kumar, L.L. Snead, P.D. Edmondson, K.G. Field, C. Silva, A. Marie Williams, K. Linton, and K.J. Leonard, LAMDA: Irradiated Materials Microscopy at Oak Ridge National Laboratory, Microsc. Microanal. 21 (2015) 1003–1004.
[32] X. Hu, T. Koyanagi, M. Fukuda, Y. Katoh, L.L. Snead, and B.D. Wirth, Defect evolution in single crystalline tungsten following low temperature and low dose neutron irradiation, J. Nucl. Mater. 470 (2016) 278–289.
[33] B.P. Eftink, G.T. Gray, and S.A. Maloy, Stereographic Methods for 3D Characterization of Dislocations, Microsc. Microanal. 23 (2017) 210–211.
[34] B. Eftink and S. Maloy, obtain3D, Computer software. Version 00. May 17, 2017.
[35] I. Dustin, P. Furrer, A. Stasiak, J. Dubochet, J. Langowski, and E. Egelman, Spatial visualization of DNA in solution, Journal of Structural Biology 107 (1991) 15–21.
[36] P. Ramachandran and G. Varoquaux, Mayavi: 3D visualization of scientific data, IEEE Comput. Sci. Eng. 13 (2011) 40–51.
[37] C.S. Becquart, C. Domain, U. Sarkar, A. DeBacker, and M. Hou, Microstructural evolution of irradiated tungsten: Ab initio parameterisation of an OKMC model, J. Nucl. Mater. 403 (2010) 75–88.
[38] W. Setyawan, G. Nandipati, K.J. Roche, H.L. Heinisch, B.D. Wirth, and R.J. Kurtz, Displacement cascades and defects annealing in tungsten, Part I: Defect database from molecular dynamics simulations, J. Nucl. Mater. 462 (2015) 329–337.
[39] A. Xu, D.E.J. Armstrong, C. Beck, M.P. Moody, G.D.W. Smith, P.A.J. Bagot, and S.G. Roberts, Ion–irradiation induced clustering in W–Re–Ta, W–Re and W–Ta alloys: An atom probe tomography and nanoindentation study, Acta Mater. 124 (2017) 71–78.
[40] T. Tanno, A. Hasegawa, M. Fujwara, J.C. He, S. Nogami, M. Satou, T. Shishido, and K. Abe, Precipitation of Solid Transmutation Elements in Irradiated Tungsten Alloys, Mater. Trans. 49 (2008) 2259–2264.
[41] H. Bolt, V. Barabash, W. Krauss, J. Linke, R. Neu, S. Suzuki, N. Yoshida, and A.U. Team, Materials for the plasma–facing components of fusion reactors, J. Nucl. Mater. 329–333 (2004) 66–73.
[42] K. Tsuchida, T. Miyazawa, A. Hasegawa, S. Nogami, and M. Fukuda, Recrystallization behavior of hot–rolled pure tungsten and its alloy plates during high–temperature annealing, Nucl. Mater. Energy 15 (2018) 158–163.

Table 1. Irradiation conditions of tungsten samples irradiated in HFIR and the calculated amount of transmutant elements

| Sample ID | Crystal structure | Irradiation Temperature (°C) | Neutron fluence ( $10^{25}$ n/m$^2$, E>0.1MeV) | Irradiation dose (dpa) | Transmutant Re (%) | Transmutant Os (%) |
|---|---|---|---|---|---|---|
| 1W47 | Single crystal (110) | 460 | 0.10 | 0.02 | 0.28 | 0.013 |
| 1W53 | Single crystal (110) | 797 | 0.46 | 0.092 | 1.2 | 0.083 |
| 1W17 | Single crystal (110) | 705 | 2.2 | 0.44 | 4.9 | 0.85 |
| 1W19 | Single crystal (110) | 770 | 9.0 | 1.8 | 9.9 | 7.3 |
| SX55 | Single crystal (110) | 1100* | 3.0 | 0.60 | 6.2 | 1.4 |
| OW158 | Polycrystalline | 800 | 7.0 | 1.5 | 9.7 | 5.7 |
| OW125 | Polycrystalline | 800 | 12 | 2.4 | 9.7 | 10.3 |

*Nominal neutron irradiation temperature without SiC temperature monitor

Table 2 Quantification of precipitates in neutron-irradiated tungsten samples.

| Samples | Defect features including transmutant elements | Average size (nm) | Number density ($m^{-3}$) |
|---|---|---|---|
| 1W47 (0.02 dpa, 460 °C) | nanoscale cluster | 4.3 | $1.8\times10^{21}$ |
| 1W53 (0.092 dpa, 797 °C) | nanoscale clusters | 5.8 | $3.6\times10^{21}$ |
| 1W17 (0.44 dpa, 705°C) | nanoscale clusters | 7.9 | $1.9\times10^{22}$ |
| 1W19 (1.8 dpa, 770°C) | Acicular shape | 23.1 | $9.0\times10^{21}$ |
| OW158 (1.5 dpa, 800°C) | Acicular shape | 24.7 | $5.0\times10^{21}$ |
| OW125 (2.4 dpa, 800°C) | Acicular shape | 30.5 | $1.0\times10^{22}$ |

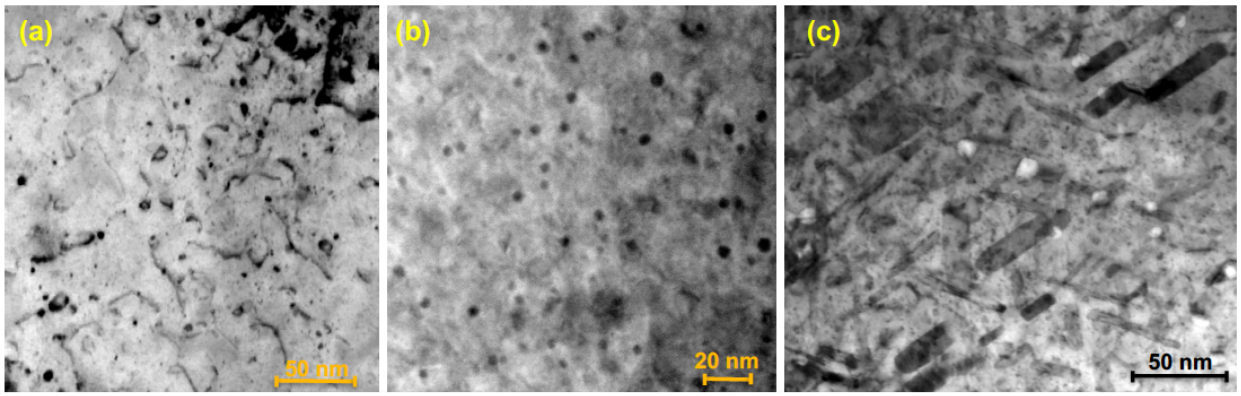


Figure 1 (a) STEM bright field and (b) high angle annular dark field (HAADF) micrograph of single crystal W irradiated at 705°C to 0.44 dpa; (c)bright field micrograph of single crystal W irradiated at 770°C to 1.80 dpa.

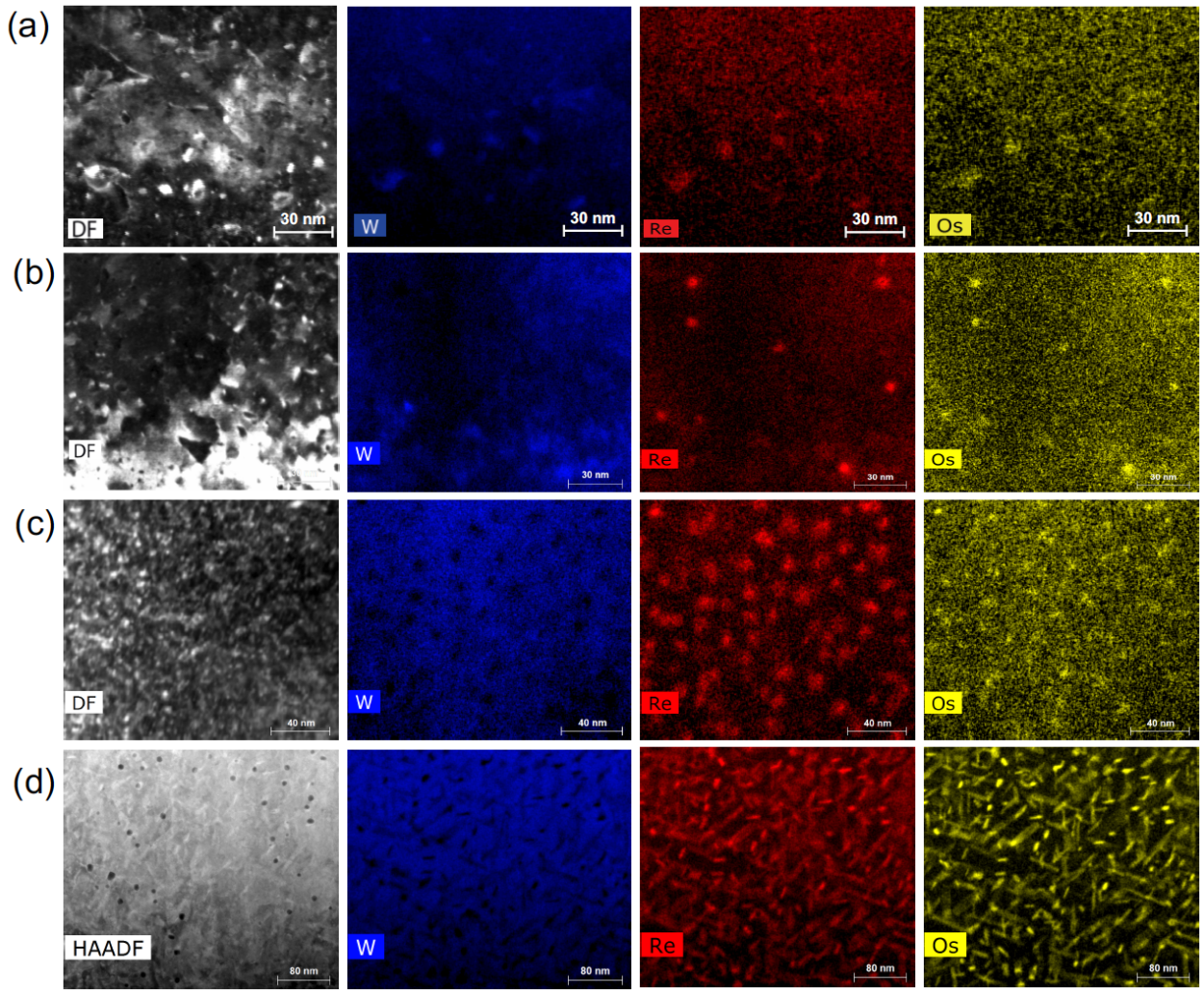


Figure 2 STEM dark field images and X-ray maps of neutron-irradiated single crystal tungsten (110): (a) 0.02dpa, 460°C; (b) 0.09dpa, 797°C; (c) 0.44 dpa, 705°C; (d) 1.80dpa, 770°C.

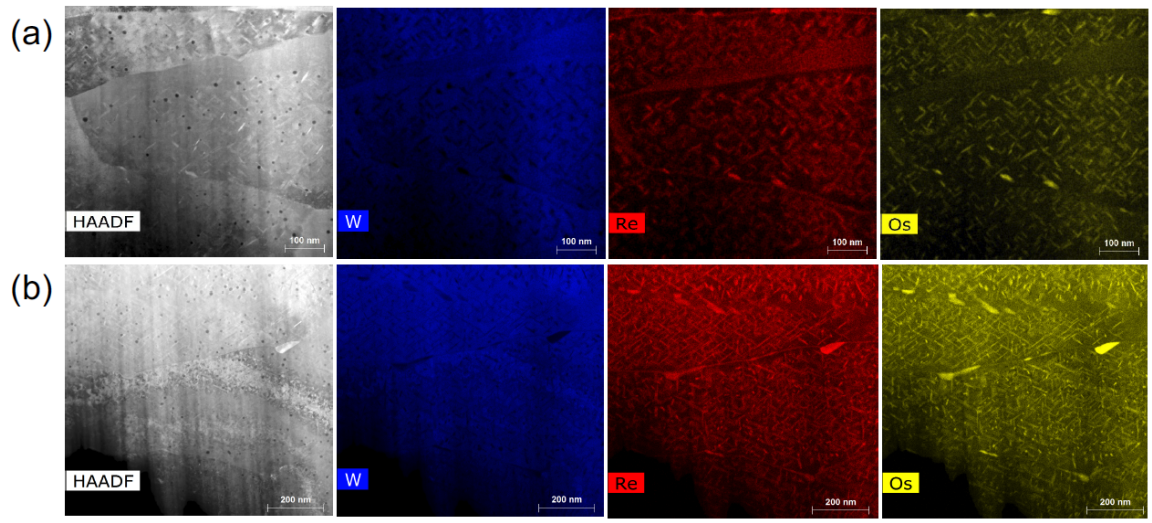


Figure 3. HADDF and X-ray maps of neutron-irradiated polycrystalline tungsten: (a) OW158 (1.5dpa, 800°C); (b) OW125 (2.4dpa, 800°C). Black dots in HADDF images refers to the voids. Microstructural features with strong bright contrasts are the precipitates. The X-ray maps showed the distribution of transmutant elements. Large precipitates were found along the grain boundaries while dense acicular precipitates were observed in the grain interiors.

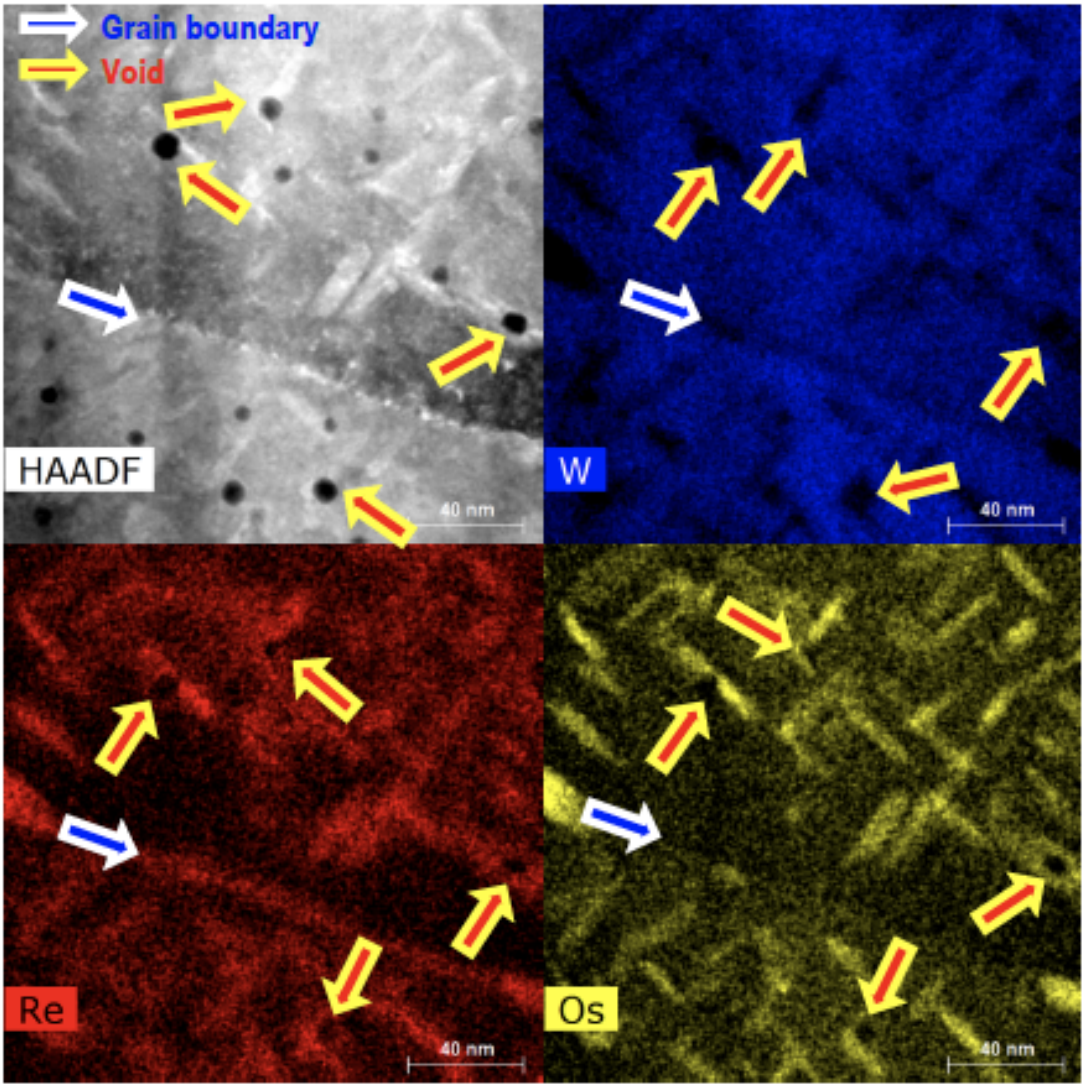


Figure 4 HAADF and X-ray maps of a local area nearby a grain boundary within OW158 (1.5 dpa, 800°C). Voids and the grain boundary are labeled using red and blue arrows, respectively. Association of voids and precipitates could be determined based on the relative positions between them.

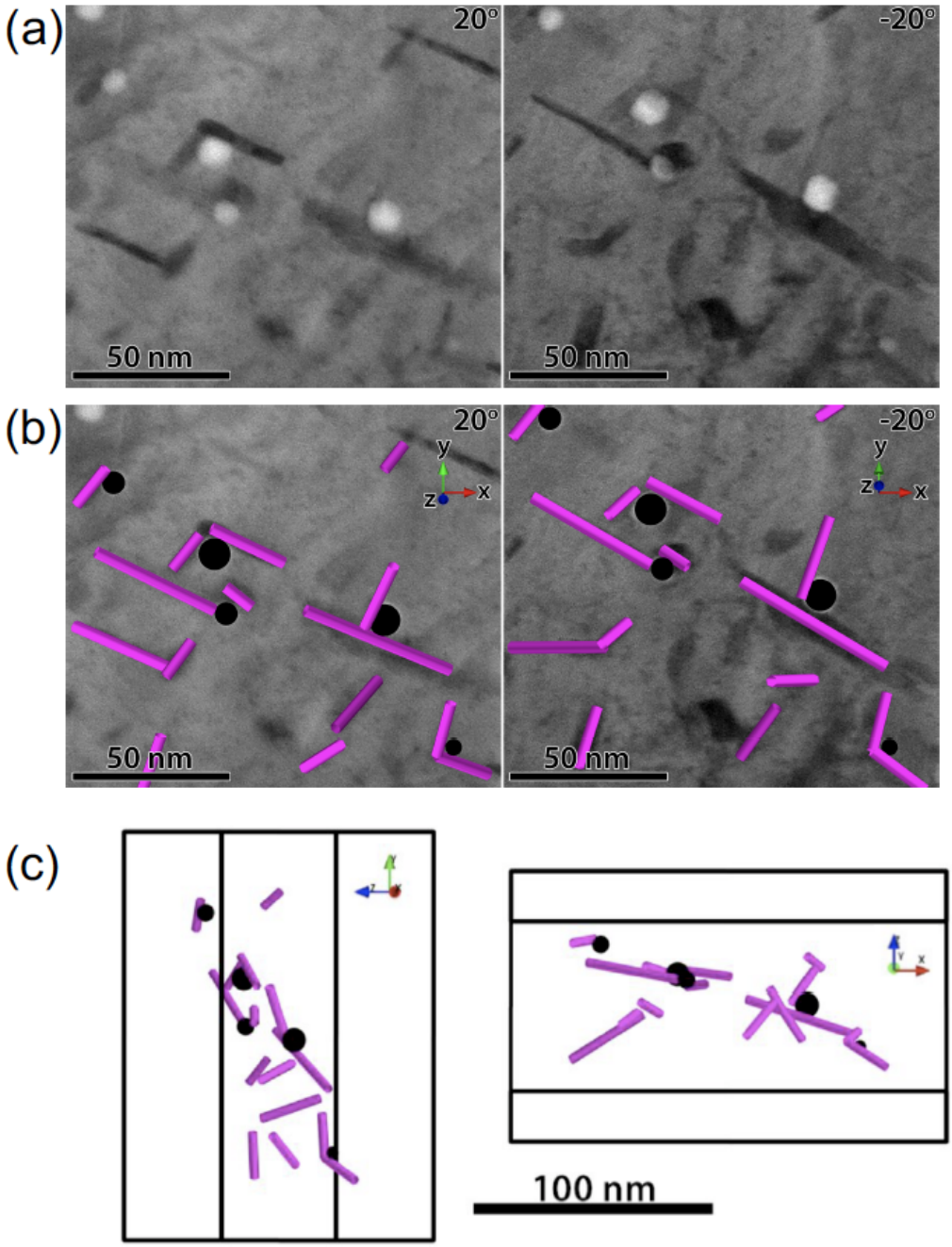


Figure 5 (a) STEM bright-field images taken at the same location of OW158 (1.5dpa, 800°C) using different sample tilts; (b) computer generated model of precipitates (purple straight lines) and voids (black circles); (c) snapshots of movie showing the correlation of precipitates and voids.

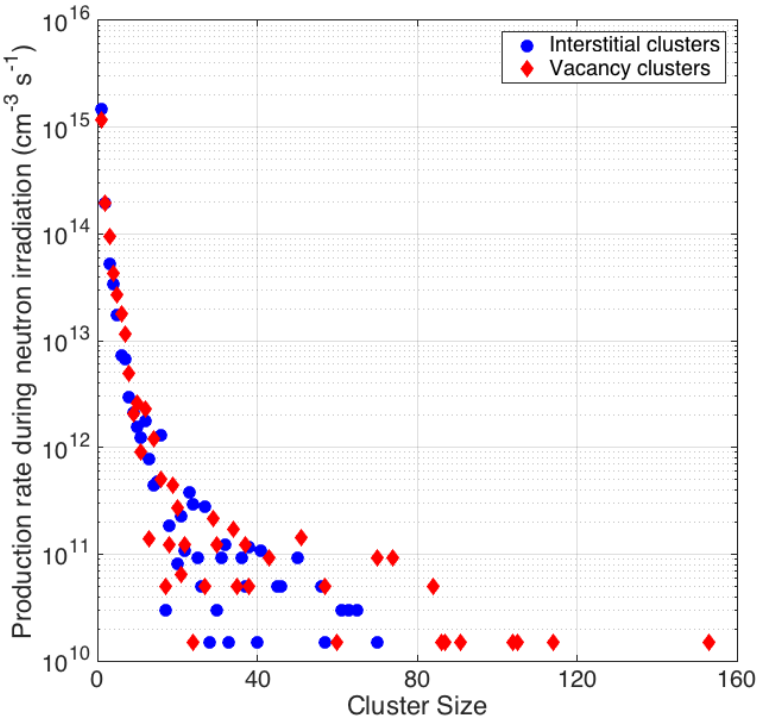


Figure 6 Defect cluster production rate in tungsten exposed to neutron irradiation in the HFIR flux trap facility

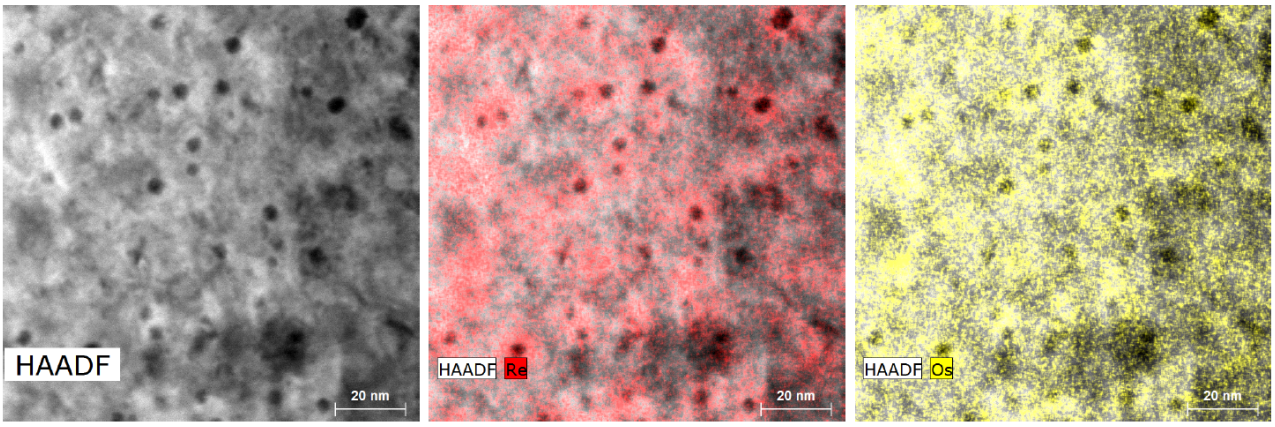

Figure 7. HAADF and EDS X-ray maps of 1W17 (0.44 dpa, 707°C)

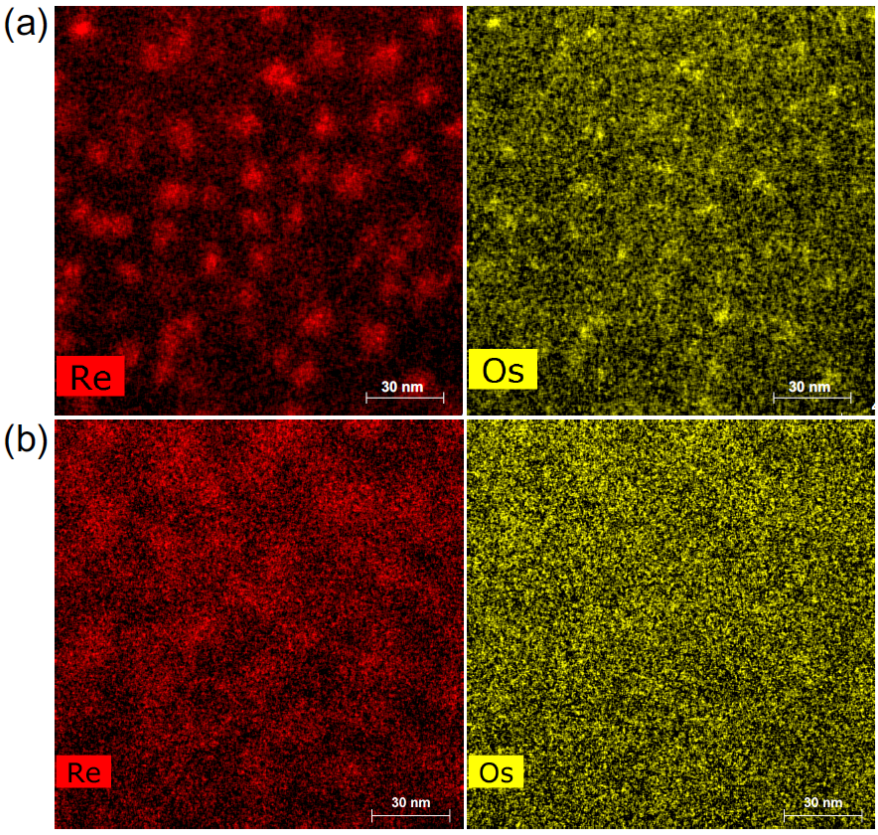


Figure 8. X-ray maps of (a) as-irradiated 1W17 (0.44 dpa, 705°C); (b) 1W17 (0.44 dpa, 705°C) following 2h annealing at 1200°C

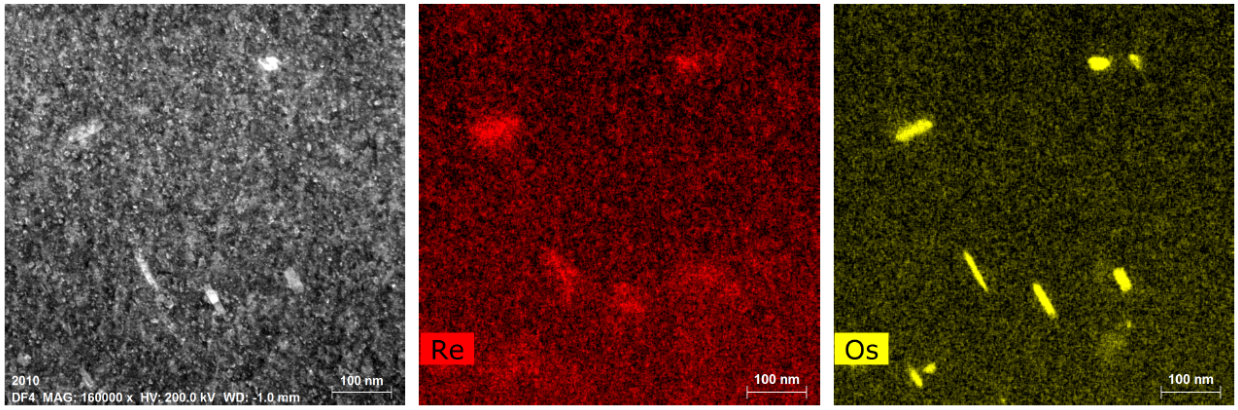

Figure 9. Dark field TEM image and X-ray maps of SX55 (0.6 dpa, 1100°C)